Commun. Comput. Phys.
doi: 10.4208/cicp.090412.121012a

Vol. **14**, No. 2, pp. 477-508
August 2013

Mathematical Modelling and Numerical Simulation of Dendrite Growth Using Phase-Field Method with a Magnetic Field Effect

A. Rasheed[1] and A. Belmiloudi[2,*]

[1] *COMSATS-IIT, Quaid Avenue, Wah Cantt, Pakistan.*
[2] *IRMAR-INSA de Rennes, 20 avenue des Buttes de Coësmes, CS 70839, 35708 Rennes Cédex 7, France.*

Received 9 April 2012; Accepted (in revised version) 12 October 2012

Available online 4 January 2013

Abstract. In this paper, we present a new model developed in order to analyze phenomena which arise in the solidification of binary mixtures using phase-field method, which incorporates the convection effects and the action of magnetic field. The model consists of flow, concentration, phase field and energy systems which are nonlinear evolutive and coupled systems. It represents the non-isothermal anisotropic solidification process of a binary mixture together with the motion in a melt with the applied magnetic field. To illustrate our model, numerical simulations of the influence of magnetic-field on the evolution of dendrites during the solidification of the binary mixture of Nickel-Copper (Ni-Cu) are developed. The results demonstrate that the dendritic growth under the action of magnetic-field can be simulated by using our model.

AMS subject classifications: 76W05, 35K55, 35R35, 74A50, 74N25, 65N30, 80A22

Key words: Modelling, Phase-field method, dendritic solidification, binary alloys, convection, magnetic-field, Magnetohydrodynamics, numerical simulations.

1 Introduction

In order to improve the quality and properties of mixtures, the major industrial challenges lie in the possibility to control the metal structure and its defects, that occur during the solidification process and then to achieve the desired properties in the final solidified metals.

*Corresponding author. *Email addresses:* amerasheed@ciitwah.edu.pk (A. Rasheed), Aziz.Belmiloudi@insa-rennes.fr, Aziz.Belmiloudi@math.cnrs.fr (A. Belmiloudi)

In recent years the so-called phase field models have become an important tool to simulate, during the solidification of pure and mixtures of materials, the formation and growth of dendrites. This approach has proved to be an emerging technology that complements experimental research. Various problems associated with phase-field formulation have been studied to treat both pure materials and binary alloys. From the theoretical or numerical simulation point view, see e.g. A. Belmiloudi et al. [5–7], D. Kessler [15], P. Laurençot [17], J. Rappaz et al. [24], S. L. Wang et al. [33] and A. A. Wheeler et al. [36]. We can note the existence of analytical solutions for this type of model, but it remains limited to very simple cases. In the case of realistic situations where the system is highly nonlinear and very complex, the numerical simulation is a necessary tool, even essential, it plays an important role in understanding and analyzing the formation of microstructures of dendrites. In this context, we can cite works of e.g., M. Grujicic et al. [10], B. Kaouil et al. [13], J. C Ramirez et al. [22, 23], M. Rappaz [25], T. Takaki et al. [29] and J. A. Warren et al. [34]. Moreover, in the last decade, the phase field method has been extended to include the effect of convection on the dendrite growth. This was motivated by the fact that during the solidification experiments it has been observed a meaningful impact of the movement in the liquid on the formation and evolution of the dendritic microstructure. For phase-field models and the simulations of dendrite growth that include the melt flow, we can cited e.g., in the case of phase-field models for the solidification of a pure metal, D. M. Anderson et al. [2] that have developed a model in which they introduced the convection using compressible Navier-Stokes equations by assuming that viscosity and density are the functions of phase-field in order to obtain the required viscosity and density variation between the two phases; R. Tonhardt et al. [31] and X. Tong al. [30] have given models by introducing convection using Navier-Stokes equations and enforcing the velocity to be zero in the solid phase. For other models which incorporate convection during the solidification, we can cite N. Al-Rawahi et al. [1], E. Bansch et al. [3]. The principle obstacle in these simulations is to compute accurately the diffusion and convection processes and to enforce the no-slip condition at the interface so that the velocity moves along-with the solid liquid interface during the solidification process.

Although significant advances in numerical simulation of microstructural evolution in the metallurgical and materials science, and therefore it is now recognized that thanks to the phase field methods, we can simulate numerically the dendritic growth in the entire domain (at the macro scale level) with actual (physically meaningful) dimensions, it still poses new and challenging problems for scientific community, because of the need to obtain approximate solutions more and more accurate and reliable. This goal can be achieved through the development of numerical analysis tools capable of reproducing fine qualitative properties and approximations of dendritic dynamics with a reasonable CPU's computation time. To reach this objective, different approaches have been recently developed, we can cite e.g. H. Wang et al. [32] in which the authors provide an *r*-adaptive moving mesh method for the quantitative phase field equations (which were provided by A. Karma et al. [14]), in both two- and three-dimensional cases. They redistribute the meshes in the physical domain by solving an optimization problem which automatically

includes the boundary conditions and solve the mesh equations by using a multigrid speedup approach. In S. Bhattacharyya et al. [8], a spectral iterative-perturbation method was developed to compute the stress distribution in polycrystalline materials with arbitrary elastic inhomogeneity and anisotropy in a multi-phase field model. For a review of the recent development of numerical methods for multi-component fluid flows with interfacial phenomena in phase-field models see e.g. J. Kim [16].

However most of these simulations show that the dendrites are deformed considerably along the melt flow but the structure of dendrites can not be controlled using these methods. More recently, experiments have been made to control the metal structure and its defects that occur, because of the non-uniform dendrites in the final product, during the solidification process to improve the quality and properties of the metals by using different means. It has shown experimentally that the microstructure of mixtures can be controlled during the solidification process by the application of magnetic field and electric current (see, e.g., Mingjun Li et al. [18]). In particular, it has been proven by different experiments that the coarse dendrites in the solidified material can be made finer, homogeneous and equiaxed to other dendrites by the application of magnetic field. For other applications of the influence of magnetic fields on the materials, we can cite, e.g., for the MHD flows H. B. Hadid et al. [12, 28], for the semi-conductor melt flow in the crystal growth A. Belmiloudi [7], M. Gunzberger et al. [11], M. Watanabe et al. [35], V. Galindo et al. [9] and for the solidification processes, J. K. Roplekar and J. A. Dantzig [26], P. J. Prescott [20] and the references therein.

To study the effect of convection and magnetic field on the evolution of micro-structure of dendrites, we have constructed a new phase-field model to simulate directional solidification and dendritic crystal growth that incorporate, among other, the convection, magnetic field and their interaction. The mathematical formulation of our model is composed of magnetohydrodynamic, concentration and phase-field systems which are time-dependent, non-linear and coupled systems in an isothermal environment. The commencing point of the present work is the two dimensional model of solidification of the binary alloys given by Warren and Boettinger [34] (they have developed a phase-field model with the state variables phase-field parameter and relative concentration of the mixtures). In order to take into account the topological changes of the micro-structure efficiently, we have included among other the effect of convection in the phase-field and solute equations in the Warren-Boettinger model and also we have introduced the equations of melt flow in the liquid phase in the presence of magnetic field which is applied externally to the entire domain. We can note that this new model, developed in the present paper, has been used in A. Belmiloudi and A. Rasheed [21] for the 2-dimensional isotropic and isothermal case. For this particular case, the existence and uniqueness results have been proved.

The paper is outlined as follows. Section 2 is concerned with the derivation of the equations governing the model. In Section 3 we give the adimensional quantities used to non-dimensionalize the model and the initial conditions of the solidification process. We discuss the numerical resolution and implementation details of the problem, then

we present numerical simulations of the dendrite growth of our model by considering different magnetic fields and compare the dendrites obtained in different simulations. Finally, conclusions are given in Section 4.

2 Mathematical modeling

2.1 Derivation of the model

Let Ω be a bounded, open, connected region of $\mathbb{R}^n$, where $n \leq 3$ is the number of space dimension, with a piecewise smooth boundary $\Gamma = \partial\Omega$ which is sufficiently regular. Initially the region Ω is occupied by a binary alloy of the solute B (e.g., Cu) in the solvent A (e.g., Ni), which is considered as incompressible electrically conducting fluid. To develop the model, first we present the derivation of the flow systems, second we give the detailed description of phase-field equation and finally the concentration and energy equations will be given.

Now we describe the flow equations. The evolution equations for the melt flow are derived from the laws of conservation of momentum and mass. The motion of the fluid is initially driven by the buoyancy force. Since the fluid is electrically conducting and also there is an applied magnetic field $\mathbf{B}$, therefore when the fluid starts moving there would be electric current. In addition to the applied magnetic field $\mathbf{B}$, there will be induced magnetic field produced by the electric currents in the liquid metal. Therefore there will be Lorentz force which acts on the fluid so that an extra body force term $\mathbf{F}$ will appear in the Navier-Stokes equations. The Lorentz force in such a flow is given by[†]

$$\mathbf{F} = \rho_e \mathbf{E} + \mathbf{J} \times \mathbf{B}, \tag{2.1}$$

where ρ_e is the electric charge density, $\mathbf{E}$ is the electric field intensity, $\mathbf{J}$ is the current density and $\mathbf{B}$ is the applied magnetic field. We assume that the walls of the domain are electric insulators and the magnetic Reynolds number is sufficiently small that the induced magnetic field is negligible as compared to the imposed magnetic field $\mathbf{B}$. The current density $\mathbf{J}$ appeared in Eq. (2.1) can be defined by the Ohm's law for the moving medium as

$$\mathbf{J} = \rho_e \mathbf{u} + \sigma_e (\mathbf{E} + \mathbf{u} \times \mathbf{B}), \tag{2.2}$$

where σ_e is electrical conductivity and $\mathbf{u}$ is the velocity of the fluid. As ρ_e is usually very small in liquid metals, therefore we shall neglect the terms $\rho_e \mathbf{E}$ and $\rho_e \mathbf{u}$ in Eqs. (2.1) and (2.2). Also as electric field is a conservative field, therefore we can express it as $\mathbf{E} = -\nabla\phi$, where ∇ is the gradient operator, ϕ is the potential function. Then the Lorentz force, given in (2.1), takes the form

$$\mathbf{F} = \sigma_e (-\nabla\phi \times \mathbf{B} + (\mathbf{u} \times \mathbf{B}) \times \mathbf{B}). \tag{2.3}$$

[†]We have assumed that the walls of the domain are electric insulators and the magnetic Reynolds number is sufficiently small that the induced magnetic field is negligible as compared to the imposed magnetic field $\mathbf{B}$.

In addition to the Ohm's law, the current density **J** is governed by the conservation of electric current, i.e., $div(\mathbf{J})=0$. Using this relation, incompressibility condition and equation (2.2), we obtain

$$\Delta\phi = div(\mathbf{u}\times\mathbf{B}), \tag{2.4}$$

where Δ is the Laplace operator and σ_e is assumed to be constant. From the above equation, we can calculate the potential function ϕ under the influence of magnetic field applied in any direction and therefore with the help of this potential along with the magnetic field **B**, we can calculate the Lorentz force **F** defined in Eq. (2.1).

Also note that to derive equations for the melt flow, we assume the Boussinesq approximations (see, e.g., [4]), as is often done in the heat and/or solute transfer problems. And as we know that the phase-field variable $\psi(\mathbf{x},t)$ is 0 in the solid phase and 1 in the liquid phase and there is no motion in the solid phase, therefore equations of the melt flow should give us the *zero* velocity in the solid region of the domain. To include this fact in the equations of melt flow, we have multiplied the Boussinesq approximation term and Lorentz force term by functions $a_1(\psi)$ and $a_2(\psi)$. These functions are chosen in way that they are 0 at $\psi=0$, so that the Boussinesq approximation term and Lorentz force term become zero in the solid region and the equations of the melt flow together with the zero initial and boundary conditions give the *zero* velocity in the solid region of the domain. Also to include the effects on the velocity with respect to the phase change variable ψ at the solid/liquid interface, we have added the term $\mathbf{f}(\psi)$ in the melt flow equations which will also be chosen so that it is *zero* at $\psi=0$. Consequently, the melt flow system can be given by using the incompressible Navier-Stokes equations with Boussinesq approximations and Lorentz force as follows

$$\begin{aligned}\rho_0\frac{D\mathbf{u}}{Dt} &= div(\vec{\sigma})+a_1(\psi)(-\beta_T T(\mathbf{x},t)-\beta_c c(\mathbf{x},t))\mathbf{G}\\ &\quad +a_2(\psi)\sigma_e(-\nabla\phi+\mathbf{u}\times\mathbf{B})\times\mathbf{B}+\alpha\mathbf{f}(\psi),\end{aligned} \tag{2.5}$$

$$div(\mathbf{u})=0, \tag{2.6}$$

where $\mathbf{x}=(x_1,x_2,x_3)$, $\mathbf{B}=(B_1,B_2,B_3)$, $D/Dt=\partial/\partial t+(\mathbf{u}\cdot\nabla)$ is the material time derivative, $\mathbf{u}=(u_1,u_2,u_3)$ is the velocity, ρ_0 is the mean density of the fluid, β_T and β_c are the thermal and solutal expansion coefficients, $\mathbf{G}=(0,0,-g)$ is the gravity vector, T(**x**,t) is the temperature, $c(\mathbf{x},t)$ is the concentration (mole fraction of the substance B in A) and $\vec{\sigma}$ is the stress tensor which is defined as

$$\vec{\sigma}=-p\mathbf{I}+\mu\left(\nabla\mathbf{u}+(\nabla\mathbf{u})^{tran}\right), \tag{2.7}$$

where p is the pressure, **I** is the unit tensor, μ is the dynamic viscosity, and *tran* represents the usual transpose of a matrix.

Remark 2.1. The functions $a_1(\psi)$ and $a_2(\psi)$ in Eq. (2.5) can be chosen, for example, as

$$a_1(\psi)=\psi, \qquad a_2(\psi)=\frac{\psi(1+\psi)}{2} \quad (\text{or } \psi).$$

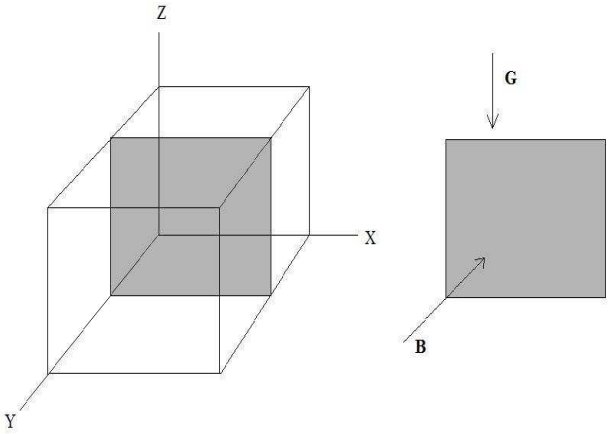

Figure 1: 2D problem description.

In order to derive the *two dimensional model*, we assume that the magnetic-field $\mathbf{B}$ and the movement are in the XZ-plane, i.e., $\mathbf{B}=(B_1,0,B_3)$, $\mathbf{u}=(u_1,0,u_3)$, $\mathbf{f}=(f_1,0,f_3)$ and all the state variables and data are not depending on the variable x_2 (see Fig. 1). Then

$$\mathbf{u}\times\mathbf{B}=(0,u_3B_1-u_1B_3,0) \quad \text{and} \quad \Delta\phi=div(\mathbf{u}\times\mathbf{B})=0.$$

Moreover, if we assume that $\nabla\phi.\mathbf{n}=0$ on the boundary of Ω (i.e. under the insulating condition on the boundary), then $\nabla\phi=0$ on Ω. We can now give the two dimensional form of the melt flow as follows (for simplicity, we shall denote $\mathbf{x}=(x,y)$, $\mathbf{u}=(u,v)$, $\mathbf{B}=(B_1,B_3)$, $\mathbf{f}=(f_1,f_3)$ and $\mathbf{G}=(0,-g)$)

$$\begin{aligned}\rho_0\frac{D\mathbf{u}}{Dt}&=div(\vec{\sigma})-a_1(\psi)(\beta_T T(\mathbf{x},t)+\beta_c c(\mathbf{x},t))\mathbf{G}\\&\quad+\sigma_e a_2(\psi)((\mathbf{u}\times\mathbf{B})\times\mathbf{B})+\alpha\mathbf{f}(\psi),\end{aligned}\tag{2.8}$$

$$div(\mathbf{u})=0,\tag{2.9}$$

where the term $(\mathbf{u}\times\mathbf{B})\times\mathbf{B}$ is defined by

$$(\mathbf{u}\times\mathbf{B})\times\mathbf{B}=\left(vB_1B_3-uB_3^2,uB_1B_3-vB_1^2\right).$$

In the next paragraph, the detailed derivation of the evolution equations for the phase-field, concentration and energy variables, will be derived. We have generalized the model of [34] and [10] by including the convection terms. Therefore we shall give a brief derivation of the evolution equations of phase-field variable, concentration and energy. These equations are based on the following entropy functional

$$S(\psi,c,e)=\int_\Omega\left(s(\psi,c,e)-\frac{\epsilon_\theta^2}{2}|\nabla\psi|^2\right)d\mathbf{x},\tag{2.10}$$

where $s(\psi,c,e)$ is an entropy density, $e(\mathbf{x},t)$ is the internal energy, $\psi(\mathbf{x},t)$ is the phase-field variable and $c(\mathbf{x},t)$ is the mole fraction of solute B in the solvent A. The second term in the integrand is a gradient entropy term analogous to the gradient energy term in the free energy, where the parameter ϵ_θ is the interfacial energy parameter which represents the gradient corrections to the entropy density.

The phase field variable $\psi(\mathbf{x},t)$ is not a conserved quantity therefore the most appropriate form of the evolution equation for the phase field is defined by

$$\frac{D\psi}{Dt} = M_\psi \frac{\delta S(\psi,c,e)}{\delta \psi}, \tag{2.11}$$

where $D/Dt = \partial/\partial t + (\mathbf{u}\cdot\nabla)$, $M_\psi > 0$ is the interfacial mobility parameter and the operator δ denotes the variational derivative. The phase field variable $\psi(\mathbf{x},t)$ varies smoothly in the interval $(0,1)$ and its value in the solid phase is 0 and in the liquid phase is 1.

The governing equations of the concentration $c(\mathbf{x},t)$ and energy $e(\mathbf{x},t)$ are derived by using conservation laws of the concentration and the energy as

$$\frac{Dc}{Dt} = -div(\mathbf{J}_c), \tag{2.12}$$

$$\frac{De}{Dt} = -div(\mathbf{J}_e), \tag{2.13}$$

where $\mathbf{J}_c$ and $\mathbf{J}_e$ are the conserved flux of concentration and energy, respectively, which can be expressed by the irreversible linear laws as

$$\mathbf{J}_c = M_c \nabla \frac{\delta S(\psi,c,e)}{\delta c}, \tag{2.14}$$

$$\mathbf{J}_e = M_e \nabla \frac{\delta S(\psi,c,e)}{\delta e}, \tag{2.15}$$

where the parameters M_c and M_e are assumed to be positive and are related to the A-B inter-diffusion coefficient and the heat conductivity, respectively, and $S(\psi,c,e)$ is the entropy functional which is defined by Eq. (2.10).

Now we need to take the variational derivative of the functional $S(\psi,c,e)$ in the sense of distribution. Let X be a topological space and U be an open set in X. Then the variational derivative of Eq. (2.10) at $\psi \in U$ in the direction of $\xi \in D(U)$ is

$$\begin{aligned}\left\langle \frac{\delta S(\psi,c,e)}{\delta \psi}, \xi \right\rangle_{D'(U),D(U)} &= \left\langle \frac{\partial s(\psi,c,e)}{\partial \psi}, \xi \right\rangle_{D'(U),D(U)} \\ &\quad - \left\langle \frac{\partial}{\partial \psi}\left(\frac{\epsilon_\theta^2}{2}|\nabla\psi|^2\right), \xi \right\rangle_{D'(U),D(U)},\end{aligned} \tag{2.16}$$

where $D'(U)$ is the space of distributions corresponding to the space $D(U)$ of test functions on U with compact support. Consider now the term

$$\mathcal{I} = \left\langle \frac{\partial}{\partial \psi}\left(\frac{\epsilon_\theta^2}{2}|\nabla\psi|^2\right), \xi \right\rangle_{D'(U),D(U)} = \int_\Omega \frac{\partial}{\partial \psi}\left(\frac{\epsilon_\theta^2}{2}|\nabla\psi|^2\right)\xi d\mathbf{x}$$

and carrying out the differentiation in the integrand on the right hand side of the above equation with respect to ψ, we have

$$\mathcal{I}=\int_\Omega\left(\epsilon_\theta|\nabla\psi|^2\frac{\partial\epsilon_\theta}{\partial\psi}\cdot\xi+\epsilon_\theta^2\nabla\psi\cdot\nabla\xi\right)d\mathbf{x}.$$

Since ϵ_θ is a function of θ, therefore by applying the chain rule and using divergence theorem, we arrive at

$$\mathcal{I}=\int_\Omega\left(\epsilon_\theta|\nabla\psi|^2\frac{\partial\epsilon_\theta}{\partial\theta}\frac{\partial\theta}{\partial\psi}\cdot\xi-div\left(\epsilon_\theta^2\nabla\psi\right)\xi\right)d\mathbf{x}. \tag{2.17}$$

Therefore the variational derivative of S can be given as

$$\frac{\delta S}{\delta\psi}=\frac{\partial s}{\partial\psi}+div\left(\epsilon_\theta^2\nabla\psi\right)-A\left(\epsilon_\theta,\epsilon_\theta',\frac{\partial\theta}{\partial\psi},\nabla\psi\right), \tag{2.18}$$

where $\epsilon_\theta'=\partial\epsilon_\theta/\partial\theta$ and $A\left(\epsilon_\theta,\epsilon_\theta',\frac{\partial\theta}{\partial\psi},\nabla\psi\right)=\epsilon_\theta\epsilon_\theta'\frac{\partial\theta}{\partial\psi}|\nabla\psi|^2$. The variational derivative of S with respect to c and e respectively, can easily be given (using (2.10)) as

$$\frac{\delta S}{\delta c}=\frac{\partial s}{\partial c}, \tag{2.19}$$

$$\frac{\delta S}{\delta e}=\frac{\partial s}{\partial e}. \tag{2.20}$$

In the above equations, the derivatives of the entropy density $s(\psi,c,e)$ with respect to ψ, c and e are left to be determined and will be calculated using free energy density $f(\psi,c,T)$. As we know from the basic thermodynamics that the free energy density can be defined by

$$f(\psi,c,T)=e(\psi,c,T)-Ts(\psi,c,e), \tag{2.21a}$$

$$\frac{1}{T}=\frac{\partial s}{\partial e}(\psi,c,e), \tag{2.21b}$$

where $e(\psi,c,T)$ and $s(\psi,c,e)$ are the internal energy density and entropy density of the binary alloy and $T(\mathbf{x},t)$ is the temperature at any point in the time-space domain. Taking the differential of the above equation we have

$$\mathrm{d}f(\psi,c,T)=\mathrm{d}e(\psi,c,T)-T\mathrm{d}s(\psi,c,e)-s(\psi,c,e)\mathrm{d}T,$$

or

$$\mathrm{d}f(\psi,c,T)=\mathrm{d}e(\psi,c,T)-T\left(\frac{\partial s}{\partial e}\mathrm{d}e+\frac{\partial s}{\partial\psi}\mathrm{d}\psi+\frac{\partial s}{\partial c}\mathrm{d}c\right)-s(\psi,c,e)\mathrm{d}T,$$

and using the definition of the temperature ($1/T=\partial s/\partial e$), the above equation takes the form

$$\mathrm{d}f(\psi,c,T)=-T\frac{\partial s}{\partial\psi}\mathrm{d}\psi-T\frac{\partial s}{\partial c}\mathrm{d}c-s\mathrm{d}T. \tag{2.22}$$

Also as we know that

$$\mathrm{d}f(\psi,c,T)=\frac{\partial f}{\partial \psi}\mathrm{d}\psi+\frac{\partial f}{\partial c}\mathrm{d}c+\frac{\partial f}{\partial T}\mathrm{d}T. \tag{2.23}$$

Comparing Eqs. (2.22) and (2.23), we have the following relations

$$\frac{\partial s(\psi,c,e)}{\partial \psi}=-\frac{1}{T}\frac{\partial f(\psi,c,T)}{\partial \psi}, \tag{2.24}$$

$$\frac{\partial s(\psi,c,e)}{\partial c}=-\frac{1}{T}\frac{\partial f(\psi,c,T)}{\partial c}, \tag{2.25}$$

$$\frac{\partial f(\psi,c,T)}{\partial T}=-s(\psi,c,e). \tag{2.26}$$

An explicit relation of the free energy density $f(\psi,c,T)$ of a binary alloy is given in [34] as

$$f(\psi,c,T)=(1-c)\mu_A(\psi,c,T)+c\mu_B(\psi,c,T), \tag{2.27}$$

where $\mu_A(\psi,c,T)$ and $\mu_B(\psi,c,T)$ are the corresponding chemical potentials of the two constituent species A and B, and are defined as

$$\mu_A(\psi,c,T)=f_A(\psi,T)+\lambda(\psi)c^2+\frac{RT}{V_m}\ln(1-c), \tag{2.28}$$

$$\mu_B(\psi,c,T)=f_B(\psi,T)+\lambda(\psi)(1-c)^2+\frac{RT}{V_m}\ln(c), \tag{2.29}$$

where $f_A(\psi,T)$ and $f_B(\psi,T)$ are the free energy densities for substances A and B respectively, R is the universal gas constant, V_m is the molar volume and $\lambda(\psi)$ is the regular solution interaction parameter associated with the enthalpy of mixing and is assumed to be

$$\lambda(\psi)=\lambda_S+p(\psi)(\lambda_L-\lambda_S),$$

where the parameters λ_S and λ_L are the enthalpies of mixing of the solid and liquid respectively. Here it is assumed that the solution is ideal (similar as in [34]), therefore the parameters λ_S and λ_L are assumed to be zero and hence $\lambda(\psi)=0$.

Now using the basic thermodynamic, the relationship for the free energy density of the pure substance can be given as

$$f_I(\psi,T)=e_I(\psi,T)-Ts_I(\psi,T),\qquad I=A\ \text{ or }\ B, \tag{2.30}$$

where $e_I(\psi,T)$ is the internal energy density and $s_I(\psi,T)$ is the entropy density of the pure substance I, with $I=A$ or B. The internal energy density for each substance is assumed to have the form in [34] as

$$e_I(\psi,T)=e_{I,S}(T)+p(\psi)(e_{I,L}(T)-e_{I,S}(T)),\quad I=A\ \text{ or }\ B, \tag{2.31}$$

where $e_{I,S}(T)$ and $e_{I,L}(T)$ are the solid and liquid internal energies of the pure substances I and are further defined as

$$e_{I,S}(T)=e_{I,S}(T_m^I)+C_S^I(T-T_m^I), \tag{2.32}$$

$$e_{I,L}(T)=e_{I,L}(T_m^I)+C_L^I(T-T_m^I), \tag{2.33}$$

where T_m^I is the melting temperature, C_S^I and C_L^I are the heat capacities of solid and liquid and $e_{I,S}(T_m^I)$ and $e_{I,L}(T_m^I)$ are the internal energies of solid and liquid at the melting temperature respectively of the substance I, where $I=A$ or B. The factor $p(\psi)$ should be selected here in the way that it is 0 in the solid phase to recover the internal energy density of solid and 1 in the liquid phase to obtain the internal energy density of the liquid for the pure substance I, that is, it should satisfy the following conditions

$$p(0)=p(1)=0, \qquad p'(\psi)>0 \quad \forall\, \psi \in]0,1[. \tag{2.34}$$

We shall elucidate further the choice of $p(\psi)$ below. The latent heat of each pure substance is defined as

$$L_I=e_{I,L}(T_m^I)-e_{I,S}(T_m^I), \qquad I=A \text{ or } B, \tag{2.35}$$

and by supposing that heat capacities are identical (*i.e.* $C_S^I=C_L^I=C_I$) for solid and liquid phase of each substance, we can write the final form of the internal energy densities of each substance using Eqs. (2.32), (2.33) and (2.35) as

$$e_I(\psi,T)=e_{I,S}(T_m^I)+C_I(T-T_m^I)+p(\psi)L_I, \qquad I=A \text{ or } B. \tag{2.36}$$

Now using Eq. (2.26), Eq. (2.30) can be written as

$$f_I(\psi,T)=e_I(\psi,T)+T\frac{\partial f_I}{\partial T}(\psi,T), \qquad I=A \text{ or } B,$$

which can further be written as

$$\frac{\partial(f_I/T)}{\partial T}+\frac{e_I(\psi,T)}{T^2}=0.$$

By integrating above equation with respect to T from T to T_m^I and using (2.36), we arrive at

$$f_I(\psi,T)=\frac{T}{T_m^I}f_I(\psi,T_m^I)+\left(e_{I,S}(T_m^I)-C_IT_m^I+L_Ip(\psi)\right)\left(1-\frac{T}{T_m^I}\right)-C_IT\ln\left(\frac{T}{T_m^I}\right). \tag{2.37}$$

Now the expression $f_I(\psi,T_m^I)$ is left only to be determined to achieve the final form of the free energy density of each substance. The choice of $f_I(\psi,T_m^I)$ is dependent on the phase field variable ψ as we should have the free energy density of the substance I in the solid phase at $\psi=0$ and in the liquid phase at $\psi=1$. Also the free energy density should be symmetric at the melting temperature with respect to $\psi=1/2$. Thus the free energy

density $f_I(\psi,T_m^I)$ that follows these conditions can be chosen as a function $g(\psi)$ of class $C^2([0,1],R)$ which satisfies the following conditions

$$\begin{cases} g(0)=g(1)=0, \\ g'(\psi)=0 \ \text{ iff } \ \psi\in\{0,1/2,1\}, \\ g''(0),\ g''(1)>0, \\ g(\psi)=g(1-\psi). \end{cases} \tag{2.38}$$

The function g can be chosen as

$$g(\psi)=\psi^2(1-\psi)^2, \tag{2.39}$$

which is a double well polynomial function of the minimum degree that satisfies the properties defined in (2.38). More details about the choice and properties of the function $g(\psi)$ can be found in [34]. Therefore the form of $f_I(\psi,T_m^I)$ is assumed to be

$$f_I(\psi,T_m^I)=T_m^I W_I\psi^2(1-\psi)^2, \tag{2.40}$$

where W_I is the constant which controls the height of the well and is defined as

$$W_I=\frac{3\sigma_I}{\sqrt{2}T_m^I\delta_I}, \qquad I=A \ \text{ or } \ B, \tag{2.41}$$

where σ_I is the solid-liquid interface energy, T_m^I is the melting temperature and δ_I is the interface thickness of the pure substance I. The graph of $f_I(\psi,T_m^I)$ is given in Fig. 2. Note that, to show that the minima of $f_I(\psi,T_m^I)$ lie only in the interval $[0,1]$, we have taken the domain interval as $[-0.5,1.5]$ for $f_I(\psi,T_m^I)$ in the figure.

Now we shall determine an expression for $p(\psi)$ by demanding that the only stable states of the system are the solid and liquid states and there are only two minima of the free energy density $f_I(\psi,T)$ at $\psi=0$ and $\psi=1$ for any temperature $T(\mathbf{x},t)$. Differentiating the relation (2.37) with respect to ψ and using (2.40), we have

$$\frac{\partial f_I(\psi,T)}{\partial\psi}=W_I T g'(\psi)+L_I p'(\psi)\left(1-\frac{T}{T_m^I}\right),$$

where $g'(\psi)=\partial g(\psi)/\partial\psi$ and $p'(\psi)=\partial p(\psi)/\partial\psi$. As $g'(0)=g'(1)=0$, we note from the above equation that $\partial f_I/\partial\psi$ is zero at $\psi=0$ and $\psi=1$ only if $p'(0)=p'(1)=0$ for any temperature $T(\mathbf{x},t)$. To ensure that the only minima of the free energy density $f_I(\psi,T)$ are at $\psi=0$ and $\psi=1$ for any temperature, the function $p(\psi)$ is required to fulfill the following conditions along with the conditions defined earlier and that it is of class $C^2([0,1],R)$

$$\begin{cases} p(0)=0,\ p(1)=1, \\ p'(0)=p'(1)=0, \\ p''(0)=p''(1)=0, \\ p'(\psi)>0, \quad \forall\ \psi\in\,]0,1[. \end{cases} \tag{2.42}$$

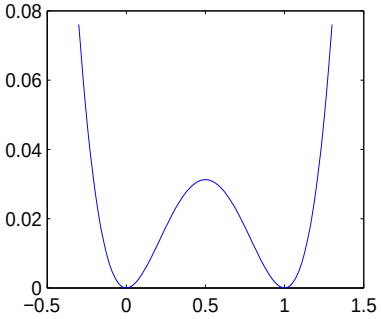

Figure 2: The graph of $f_I(\psi,T_m^I)$.

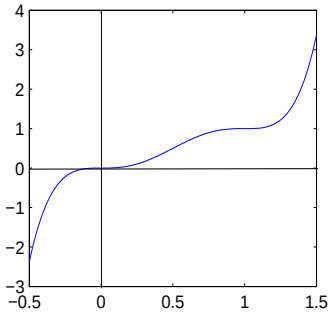

Figure 3: The graph of function $p(\psi)$.

This function can be chosen as (see, e.g., [34])

$$p(\psi)=\psi^3\left(10-15\psi+6\psi^2\right) \quad \text{such that} \quad p'(\psi)=30g(\psi), \tag{2.43}$$

which satisfies the conditions defined in (2.42). The graph of the function $p(\psi)$ is given in Fig. 3. Note that, to show the behavior of the function $p(\psi)$ within the interval $[0,1]$, we have taken the domain interval as $[-0.5,1.5]$.

Thus the final form of the free energy density for the substance I, where $I=A$ or B, can be given as

$$f_I(\psi,T)=W_I T g(\psi)+\left(e_{I,S}(T_m^I)-C_I T_m^I+L_I p(\psi)\right)\left(1-\frac{T}{T_m^I}\right)-C_I T\ln\left(\frac{T}{T_m^I}\right). \tag{2.44}$$

Now using the relations (2.27)-(2.29) in Eq. (2.24), we have

$$\frac{\partial s}{\partial\psi}=-\frac{1}{T}\frac{\partial}{\partial\psi}\left\{(1-c)\left(f_A(\psi,T)+\frac{RT}{V_m}ln(1-c)\right)\right\}+\frac{1}{T}\frac{\partial}{\partial\psi}\left\{c\left(f_B(\psi,T)+\frac{RT}{V_m}\ln(c)\right)\right\},$$

where $\lambda(\psi)=0$.

Using (2.44) and carrying out the differentiation with respect to ψ, we have

$$\begin{aligned}\frac{\partial s}{\partial\psi}=&-\frac{1}{T}(1-c)\left(W_A g'(\psi)T+p'(\psi)L_A\left(1-\frac{T}{T_m^A}\right)\right)\\&-\frac{1}{T}c\left(W_B g'(\psi)T+p'(\psi)L_B\left(1-\frac{T}{T_m^B}\right)\right).\end{aligned}$$

The above equation can be written as

$$\frac{\partial s}{\partial\psi}=-(1-c)H_A(\psi,T)-cH_B(\psi,T), \tag{2.45}$$

where (since $p'(\psi)=30g(\psi)$)

$$H_A(\psi,T)=W_Ag'(\psi)+30g(\psi)L_A\left(\frac{1}{T}-\frac{1}{T_m^A}\right), \tag{2.46}$$

$$H_B(\psi,T)=W_Bg'(\psi)+30g(\psi)L_B\left(\frac{1}{T}-\frac{1}{T_m^B}\right), \tag{2.47}$$

where $g'(\psi)=\partial g(\psi)/\partial\psi$.

Substituting Eq. (2.45) into Eq. (2.18) and then the resulting equation in Eq. (2.11), we obtain the following equation

$$\frac{D\psi}{Dt}=M_\psi\Big(div\left(\epsilon_\theta^2\nabla\psi\right)-(1-c)H_A(\psi,T)-cH_B(\psi,T)-A\Big(\epsilon_\theta,\epsilon_\theta',\frac{\partial\theta}{\partial\psi},\nabla\psi\Big)\Big), \tag{2.48}$$

which is the general equation of phase-field, where the operators A and $div\left(\epsilon_\theta^2\nabla\psi\right)$ are left to be calculated. We can compute these operators by introducing the operator ϵ_θ.

In *two dimensional geometry*, the parameter ϵ_θ is assumed to be anisotropic and is defined as [34]

$$\epsilon_\theta=\epsilon_0\eta=\epsilon_0(1+\gamma_0\cos k\theta), \tag{2.49}$$

where anisotropic means that ϵ_θ is dependent on the direction of the solid-liquid interface, γ_0 is the anisotropic amplitude, k the mode number, ϵ_0 is a constant and

$$\theta=\arctan\left(\frac{\psi_y}{\psi_x}\right), \tag{2.50}$$

is the angle between the local interface normal and a designated base vector of the crystal lattice, subscripts x and y are used to denote the partial derivatives with respect to spatial coordinates, that is, $\psi_x=\partial\psi/\partial x$ and $\psi_y=\partial\psi/\partial y$.

Remark 2.2. The anisotropy plays an important role in modeling the dendritic solidification process. In fact, for example, for the metal alloys, the form of dendrites is usually symmetric and has four major dendrite arms and minor arms around them. In the solidification model, the mode number k, in the anisotropy function ϵ_θ, usually represents the dendrite arms. If we want to obtain a dendrite with four arms, we fix the value of k equal to 4. Its value depends on the form of dendrites obtained in a particular alloy.

By calculating the operators A and $div\left(\epsilon_\theta^2\nabla\psi\right)$ (according to the expression of ϵ_θ and θ, we can deduce, from (2.48), the following two dimensional model

$$\begin{aligned}\frac{D\psi}{Dt}=&M_\psi\left(\epsilon_0^2\eta^2\Delta\psi-(1-c)H_A(\psi,T)-cH_B(\psi,T)\right)\\&-\frac{M_\psi\epsilon_0^2\left(\eta\eta''+(\eta')^2\right)}{2}\left\{2\psi_{xy}\sin2\theta-\Delta\psi-\left(\psi_{yy}-\psi_{xx}\right)\cos2\theta\right\}\\&+M_\psi\epsilon_0^2\eta\eta'\left\{\sin2\theta\left(\psi_{yy}-\psi_{xx}\right)+2\psi_{xy}\cos2\theta\right\},\end{aligned} \tag{2.51}$$

which is the final form of the evolution equation for the phase-field $\psi(\mathbf{x},t)$, where we assume M_ψ to be a positive constant.

If we assume that the interface thickness $\delta_A=\delta_B=\delta$ in the parameters defined in the relation (2.41), then Eq. (2.51) can be simplified and takes the form

$$\begin{aligned}\frac{D\psi}{Dt}=&M_\psi\epsilon_0^2\left(\eta^2\Delta\psi-\frac{\lambda_1(c)}{\delta^2}g'(\psi)-\frac{1}{\delta}\lambda_2(c)p'(\psi)\right)\\&-\frac{M_\psi\epsilon_0^2\left(\eta\eta''+(\eta')^2\right)}{2}\Big\{2\psi_{xy}\sin2\theta-\Delta\psi-\left(\psi_{yy}-\psi_{xx}\right)\cos2\theta\Big\}\\&+M_\psi\epsilon_0^2\eta\eta'\Big\{\sin2\theta\left(\psi_{yy}-\psi_{xx}\right)+2\psi_{xy}\cos2\theta\Big\},\end{aligned}\tag{2.52}$$

where

$$\epsilon_0^2=\frac{3\sqrt{2}(\sigma_A+\sigma_B)\delta}{T_m},\qquad T_m=\frac{T_m^A+T_m^B}{2},\tag{2.53a}$$

$$\lambda_1(c)=(1-c)\lambda_{1A}+c\lambda_{1B},\quad \lambda_2(c)=(1-c)\lambda_{2A}+c\lambda_{2B},\tag{2.53b}$$

with

$$\lambda_{1A}=\frac{\sigma_A}{(\sigma_A+\sigma_B)}\frac{T_m}{T_m^A},\qquad \lambda_{1B}=\frac{\sigma_B}{(\sigma_A+\sigma_B)}\frac{T_m}{T_m^B},$$

$$\lambda_{2A}=\frac{L_AT_m}{3\sqrt{2}(\sigma_A+\sigma_B)}\left(\frac{1}{T}-\frac{1}{T_m^A}\right),\quad \lambda_{2B}=\frac{L_BT_m}{3\sqrt{2}(\sigma_A+\sigma_B)}\left(\frac{1}{T}-\frac{1}{T_m^A}\right).$$

Now we present the derivation of the concentration and energy equations. It is observed by Warren and Boettinger [34] that the terms ∇T in the concentration equation (2.12) and ∇c in the energy equation (2.13) are the small corrections. Therefore, in the derivation of the concentration equation, we shall assume that the temperature $T(\mathbf{x},t)$ is constant and in the derivation of energy equation, the concentration $c(\mathbf{x},t)$ will be assumed fixed.

By employing Eqs. (2.27), (2.25) and (2.19), Eq. (2.14) takes the form

$$\mathbf{J}_c=M_c\nabla\left(-\frac{\mu_B(\psi,c,T)-\mu_A(\psi,c,T)}{T(\mathbf{x},t)}\right).$$

Since temperature $T(\mathbf{x},t)$ is assumed to be constant, therefore the above equation can be written as

$$\mathbf{J}_c=-\frac{M_c}{T}\nabla\left(\mu_B(\psi,c,T)-\mu_A(\psi,c,T)\right).$$

With the help of Eqs. (2.28) and (2.29), the above equation takes the form

$$\begin{aligned}\mathbf{J}_c=&-\frac{M_c}{T}\left(\nabla f_B(\psi,T)+\frac{RT}{V_m}\frac{1}{c}\nabla c\right)\\&+\frac{M_c}{T}\left(\nabla f_A(\psi,T)+\frac{RT}{V_m}\frac{1}{1-c}(-\nabla c)\right).\end{aligned}$$

Making use of the relation (2.44), we obtain

$$\begin{aligned}\mathbf{J}_c = M_c\left(-W_B g'(\psi) - p'(\psi)L_B\left(\frac{1}{T}-\frac{1}{T_m^B}\right)\right)\nabla\psi \\ + M_c\left(W_A g'(\psi) + p'(\psi)L_A\left(\frac{1}{T}-\frac{1}{T_m^A}\right)\right)\nabla\psi \\ + M_c\left(-\frac{R}{V_m}\frac{1}{c}\nabla c - \frac{R}{V_m}\frac{1}{1-c}(\nabla c)\right).\end{aligned}$$

Using the relations (2.46) and (2.47) in the above equation, we have

$$\mathbf{J}_c = M_c(H_A(\psi,T)-H_B(\psi,T))\nabla\psi - \frac{M_c R}{V_m c(1-c)}\nabla c. \tag{2.54}$$

Also the comparison of Eq. (2.54) with the Fick's first law in a single-phase system (i.e., with $\nabla\psi = 0$) establishes the relation given below [34]

$$M_c = D(\psi)\frac{V_m c(1-c)}{R}, \tag{2.55}$$

where $D(\psi) = D_S + p(\psi)(D_L - D_S)$ is the A-B inter-diffusion coefficient.

Substituting (2.55) into Eq. (2.54), we obtain

$$\mathbf{J}_c = D(\psi)\frac{V_m c(1-c)}{R}(H_A(\psi,T)-H_B(\psi,T))\nabla\psi - D(\psi)\nabla c. \tag{2.56}$$

Finally substituting Eq. (2.56) into Eq. (2.12), we have

$$\frac{Dc}{Dt} = div\left(D(\psi)\left(\nabla c + \frac{c(1-c)V_m}{R}(H_B(\psi,T)-H_A(\psi,T))\nabla\psi\right)\right). \tag{2.57}$$

Eq. (2.57) represents the final form of the evolution equation for the mole fraction (concentration) of the solute.

If we assume that the interface thickness $\delta_A = \delta_B = \delta$ in the parameters defined in the expression (2.41), then the above equation reduces to the following equation

$$\frac{Dc}{Dt} = div(D(\psi)\nabla c) + div\left(\alpha_0 D(\psi)c(1-c)\left\{\frac{1}{\delta}\lambda_1'(c)g'(\psi) + \lambda_2'(c)p'(\psi)\right\}\nabla\psi\right), \tag{2.58}$$

where

$$\alpha_0 = \frac{3\sqrt{2}V_m}{RT_m}(\sigma_A + \sigma_B), \tag{2.59}$$

with $\lambda_1'(c) = \partial\lambda(c)/\partial c$, $\lambda_2'(c) = \partial\lambda(c)/\partial c$, where $\lambda_1(c)$ and $\lambda_2(c)$ are defined in (2.53).

For the derivation of the evolution equation for the energy, first, the internal energy density of a binary alloy can be expressed using a rule of mixture as (e.g., [10])

$$e(\psi,c,T) = (1-c)e_A(\psi,T) + c\, e_B(\psi,T). \tag{2.60}$$

Using the definition of the temperature $\partial s/\partial e = 1/T$ into Eqs. (2.20) and (2.15) we get

$$\mathbf{J}_e = M_e\left(-\frac{1}{T^2}\nabla T(\mathbf{x},t)\right). \tag{2.61}$$

Now substituting (2.60) and (2.61) in Eq. (2.13), we have

$$\frac{D}{Dt}((1-c)e_A(\psi,T)+c\,e_B(\psi,T)) = -\nabla\cdot\left(M_e\left(-\frac{1}{T^2}\nabla T(\mathbf{x},t)\right)\right).$$

Since concentration $c(\mathbf{x},t)$ is considered constant in the derivation of the energy equation, therefore the above equation takes the form

$$(1-c)\frac{De_A(\psi,T)}{Dt}+c\,\frac{De_B(\psi,T)}{Dt} = -\nabla\cdot\left(M_e\left(-\frac{1}{T^2}\nabla T(\mathbf{x},t)\right)\right).$$

By using (2.36) and setting $M_e = KT^2$, where K is the thermal conductivity, the above equation becomes

$$(1-c)\left(C_A\frac{DT}{Dt}+L_A\frac{Dp(\psi)}{Dt}\right)+c\,\left(C_B\frac{DT}{Dt}+L_B\frac{Dp(\psi)}{Dt}\right) = \nabla\cdot(K\nabla T).$$

Applying chain rule and re-arranging the above equation, we have

$$((1-c)C_A+cC_B)\frac{DT}{Dt}+((1-c)L_A+cL_B)p'(\psi)\frac{D\psi}{Dt} = \nabla\cdot(K\nabla T).$$

Further the above equation can be written as

$$C\frac{DT(\mathbf{x},t)}{Dt}+30L\,g(\psi)\frac{D\psi(\mathbf{x},t)}{Dt} = \nabla\cdot(K\nabla T(\mathbf{x},t)), \tag{2.62}$$

where

$$\begin{aligned} C &= (1-c)C_A+cC_B,\\ L &= (1-c)L_A+cL_B,\\ K &= (1-c)K_A+cK_B, \end{aligned}$$

with K_A and K_B, the thermal conductivities of substances A and B respectively. Eq. (2.62) represents the final form of the evolution equation for the temperature field $T(\mathbf{x},t)$.

We can now summarize the governing equations of the model.

2.2 The governing equations of the model

2.2.1 General model

In this section, we shall summarize the entire set of governing equations that model the solidification process of a binary alloy in a non-isothermal environment in the presence of motion in the liquid phase with the magnetic field effect. The equations that model this phenomenon are the phase-field equation (2.48), concentration equation (2.57), energy equation (2.62) and the melt flow system (2.4), (2.5) and (2.6) which are given below

$$\rho_0\frac{D\mathbf{u}}{Dt}=div(\vec{\sigma})+a_1(\psi)(-\beta_T T(\mathbf{x},t)-\beta_c c(\mathbf{x},t))\mathbf{G} + a_2(\psi)\sigma_e(-\nabla\phi+\mathbf{u}\times\mathbf{B})\times\mathbf{B}+\alpha\mathbf{f}(\psi) \text{ on } \mathcal{Q}, \tag{2.63a}$$

$$div(\mathbf{u})=0 \text{ on } \mathcal{Q}, \tag{2.63b}$$

$$\frac{D\psi}{Dt}=M_\psi\left(div\left(\epsilon_\theta^2\nabla\psi\right)-(1-c)H_A(\psi,T)-cH_B(\psi,T)-A\left(\epsilon_\theta,\epsilon_\theta',\frac{\partial\theta}{\partial\psi},\nabla\psi\right)\right) \text{ on } \mathcal{Q}, \tag{2.63c}$$

$$\frac{Dc}{Dt}=div\left(D(\psi)\left(\nabla c+\frac{c(1-c)V_m}{R}(H_B(\psi,T)-H_A(\psi,T))\nabla\psi\right)\right) \text{ on } \mathcal{Q}, \tag{2.63d}$$

$$C\frac{DT}{Dt}+30L\,g(\psi)\frac{\partial\psi}{\partial t}=\nabla\cdot(K\nabla T) \text{ on } \mathcal{Q}, \tag{2.63e}$$

$$\Delta\phi=div(\mathbf{u}\times\mathbf{B}) \text{ on } \mathcal{Q}, \tag{2.63f}$$

where $\vec{\sigma}=-p\mathbf{I}+\mu\left(\nabla\mathbf{u}+(\nabla\mathbf{u})^{tran}\right)$, $\mathcal{Q}=\Omega\times\left(0,T_f\right)$, T_f is the solidification time and the expressions for the nonlinear operators and for the parameters are defined earlier. In the case of an isothermal process, the model (2.63) can be reduced to

$$\rho_0\frac{D\mathbf{u}}{Dt}=div(\vec{\sigma})-a_1(\psi)\beta_c c(\mathbf{x},t)\mathbf{G}+a_2(\psi)\sigma_e(-\nabla\phi+\mathbf{u}\times\mathbf{B})\times\mathbf{B}+\alpha\tilde{\mathbf{f}}(\psi) \text{ on } \mathcal{Q}, \tag{2.64a}$$

$$div(\mathbf{u})=0 \text{ on } \mathcal{Q}, \tag{2.64b}$$

$$\frac{D\psi}{Dt}=M_\psi\left(div\left(\epsilon_\theta^2\nabla\psi\right)-(1-c)\tilde{H}_A(\psi)-c\tilde{H}_B(\psi)-A\left(\epsilon_\theta,\epsilon_\theta',\frac{\partial\theta}{\partial\psi},\nabla\psi\right)\right) \text{ on } \mathcal{Q}, \tag{2.64c}$$

$$\frac{Dc}{Dt}=div\left(D(\psi)\left(\nabla c+\frac{c(1-c)V_m}{R}\left(\tilde{H}_B(\psi)-\tilde{H}_A(\psi)\right)\nabla\psi\right)\right) \text{ on } \mathcal{Q}, \tag{2.64d}$$

$$\Delta\phi=div(\mathbf{u}\times\mathbf{B}) \text{ on } \mathcal{Q}, \tag{2.64e}$$

where

$$\tilde{\mathbf{f}}(\psi)=-\frac{a_1(\psi)\beta_T T\mathbf{G}}{\alpha}+\mathbf{f}(\psi) \quad \text{and} \quad \tilde{H}_I(\psi)=H_I(\psi,T)$$

for $I=A,B$.

Next we shall reduce the previous systems to the two dimensional geometry.

2.2.2 Two dimensional geometry

In a two dimensional case, we have worked in the XZ-plane and we have supposed that $\nabla\phi.\mathbf{n}=0$ on the boundary of the solidification domain Ω. According to (2.8), (2.49), (2.50) and (2.51), the two dimensional model is

$$\rho_0\frac{D\mathbf{u}}{Dt}=div(\vec{\sigma})+a_1(\psi)\left(-\beta_T T(\mathbf{x},t)-\beta_c c(\mathbf{x},t)\right)\mathbf{G} +a_2(\psi)\sigma_e(\mathbf{u}\times\mathbf{B})\times\mathbf{B}+\alpha\mathbf{f}(\psi) \text{ on } \mathcal{Q}, \tag{2.65a}$$

$$div(\mathbf{u})=0 \text{ on } \mathcal{Q}, \tag{2.65b}$$

$$\frac{D\psi}{Dt}=M_\psi\left(\epsilon_0^2\eta^2\Delta\psi-(1-c)H_A(\psi,T)-cH_B(\psi,T)\right) -\frac{M_\psi\epsilon_0^2\left(\eta\eta''+(\eta')^2\right)}{2}\left\{2\psi_{xy}\sin2\theta-\Delta\psi-\left(\psi_{yy}-\psi_{xx}\right)\cos2\theta\right\} +M_\psi\epsilon_0^2\eta\eta'\left\{\sin2\theta\left(\psi_{yy}-\psi_{xx}\right)+2\psi_{xy}\cos2\theta\right\} \text{ on } \mathcal{Q}, \tag{2.65c}$$

$$\frac{Dc}{Dt}=div\left(D(\psi)\left(\nabla c+\frac{c(1-c)V_m}{R}\left(H_B(\psi,T)-H_A(\psi,T)\right)\nabla\psi\right)\right) \text{ on } \mathcal{Q}, \tag{2.65d}$$

$$C\frac{DT}{Dt}+30L\,g(\psi)\frac{\partial\psi}{\partial t}=\nabla\cdot(K\nabla T) \text{ on } \mathcal{Q}. \tag{2.65e}$$

In the case of an isothermal process, the model (2.65) is reduced to

$$\rho_0\frac{D\mathbf{u}}{Dt}=div(\vec{\sigma})-a_1(\psi)\beta_c c(\mathbf{x},t)\mathbf{G}+a_2(\psi)\sigma_e(\mathbf{u}\times\mathbf{B})\times\mathbf{B}+\alpha\tilde{\mathbf{f}}(\psi) \text{ on } \mathcal{Q}, \tag{2.66a}$$

$$div(\mathbf{u})=0 \text{ on } \mathcal{Q}, \tag{2.66b}$$

$$\frac{D\psi}{Dt}=M_\psi\left(\epsilon_0^2\eta^2\Delta\psi-(1-c)\tilde{H}_A(\psi)-c\tilde{H}_B(\psi)\right) -\frac{M_\psi\epsilon_0^2\left(\eta\eta''+(\eta')^2\right)}{2}\left\{2\psi_{xy}\sin2\theta-\Delta\psi-\left(\psi_{yy}-\psi_{xx}\right)\cos2\theta\right\} +M_\psi\epsilon_0^2\eta\eta'\left\{\sin2\theta\left(\psi_{yy}-\psi_{xx}\right)+2\psi_{xy}\cos2\theta\right\} \text{ on } \mathcal{Q}, \tag{2.66c}$$

$$\frac{Dc}{Dt}=div\left(D(\psi)\left(\nabla c+\frac{c(1-c)V_m}{R}\left(\tilde{H}_B(\psi)-\tilde{H}_A(\psi)\right)\nabla\psi\right)\right) \text{ on } \mathcal{Q}. \tag{2.66d}$$

Nota Bene: In the sequel, we omit the " ˜ " in the system (2.66).

We assume that there exists a unique solution $(\mathbf{u},\psi,c)$ of the problem (2.66), under some hypotheses for data and some regularity of the nonlinear operators. In particular, for the isotropic case of the model (2.66), we have proved the existence and the uniqueness results in [21]. In the next section, we shall present the numerical simulations of the dendrite growth during the solidification of a Ni-Cu (Nickel-Copper) binary mixture. To perform these simulations, we consider the two dimensional and isothermal model (2.66). We further suppose that the interface thicknesses for both substances are equal i.e., $\delta_A=\delta_B=\delta$.

3 Numerical study

For the numerical simulations of dendrite growth during the solidification process, we have considered the isothermal model, that is, the energy equation is not included in the simulations. Also we have considered the simplified case by assuming $\delta_A=\delta_B=\delta$. According to (2.66) with the relations (2.46), (2.47) and (2.53), the complete set of equations can be given by

$$\rho_0\frac{D\mathbf{u}}{Dt}=div(\vec{\sigma})-a_1(\psi)\beta_c c(\mathbf{x},t)\mathbf{G}+a_2(\psi)\sigma_e(\mathbf{u}\times\mathbf{B})\times\mathbf{B}+\alpha\mathbf{f}(\psi)\quad\text{on }\mathcal{Q}, \tag{3.1a}$$

$$div(\mathbf{u})=0\quad\text{on }\mathcal{Q}, \tag{3.1b}$$

$$\begin{aligned}\frac{D\psi}{Dt}=&M_\psi\epsilon_0^2\left(\eta^2\Delta\psi-\frac{\lambda_1(c)}{\delta^2}g'(\psi)-\frac{\lambda_2(c)}{\delta}p'(\psi)\right)\\&-\frac{M_\psi\epsilon_0^2\left(\eta\eta''+(\eta')^2\right)}{2}\left\{2\psi_{xy}\sin2\theta-\Delta\psi-\left(\psi_{yy}-\psi_{xx}\right)\cos2\theta\right\}\\&+M_\psi\epsilon_0^2\eta\eta'\left\{\sin2\theta\left(\psi_{yy}-\psi_{xx}\right)+2\psi_{xy}\cos2\theta\right\}\quad\text{on }\mathcal{Q},\end{aligned} \tag{3.1c}$$

$$\begin{aligned}\frac{Dc}{Dt}=&div(D(\psi)\nabla c)+div\left(\alpha_0 D(\psi)c(1-c)\left(\frac{\lambda_1'(c)}{\delta}g'(\psi)\right.\right.\\&\left.\left.-\lambda_2'(c)p'(\psi)\right)\nabla\psi\right)\quad\text{on }\mathcal{Q}.\end{aligned} \tag{3.1d}$$

We suppose that the physical system, where solidification process takes place, is a closed system, that is, there is no phase and concentration exchange across the boundary and the velocity in the liquid phase along the boundary is negligible. Therefore we have enclosed the system by taking Neumann boundary conditions for the phase-field and concentration variables and no-slip condition for the velocity along with the initial conditions given below

$$(\mathbf{u},\psi,c)(t=0)=(\mathbf{u}_0,\psi_0,c_0)\quad\text{on }\Omega, \tag{3.2a}$$

$$\mathbf{u}=0,\quad\frac{\partial\psi}{\partial\mathbf{n}}=\nabla\psi\cdot\mathbf{n}=0,\quad\frac{\partial c}{\partial\mathbf{n}}=\nabla c\cdot\mathbf{n}=0\quad\text{on }\Sigma=\partial\Omega\times\left(0,T_f\right), \tag{3.2b}$$

where $\mathbf{n}$ is the unit outward normal to the boundary $\partial\Omega$.

In the next section, we shall present the non-dimensionalization and the details of the physical parameters used in the simulations of the model (3.1)-(3.2).

3.1 Non-dimensionalization and parameter details

We have non-dimensionalize the model (3.1) by introducing the following dimensionless quantities

$$\tilde{\mathbf{x}}=\frac{\mathbf{x}}{\ell},\quad\tilde{t}=\frac{D_L t}{\ell^2},\quad\tilde{\mathbf{u}}(\tilde{\mathbf{x}},\tilde{t})=\frac{\ell}{D_L}\mathbf{u}(\mathbf{x},t),\quad\tilde{p}=\frac{\ell^3}{D_L^2}p,$$

$$\tilde{\mathbf{B}}=\frac{\mathbf{B}}{B_0},\quad \tilde{\psi}(\tilde{\mathbf{x}},\tilde{t})=\psi(\mathbf{x},t),\quad \tilde{c}(\tilde{\mathbf{x}},\tilde{t})=c(\mathbf{x},t), \tag{3.3}$$

where $\tilde{\mathbf{x}}$ and $\tilde{t}$ are the dimensionless spatial and time coordinates, $\tilde{\mathbf{u}}$, $\tilde{\psi}$, and $\tilde{c}$ are the nondimensional velocity-field, phase-field and concentration respectively, ℓ is the characteristic length of the domain Ω, ℓ^2/D_L is the liquid diffusion time, D_L is the solutal diffusivity in liquid and B_0 is the characteristic magnetic-field. Note that the phase-field is a mathematical quantity and c is the relative concentration which are already dimensionless quantities. Using these adimensional relations, we get finally the dimensionless form of the model as

$$\begin{aligned}\frac{D\tilde{\mathbf{u}}}{D\tilde{t}}=&\tilde{div}(-p\mathbf{I}+Pr(\tilde{\nabla}\tilde{\mathbf{u}}+(\tilde{\nabla}\tilde{\mathbf{u}})^{tran})+PrRa_c a_1(\tilde{\psi})\tilde{c}\mathbf{e}_G\\&+Pr(Ha)^2a_2(\tilde{\psi})(\tilde{\mathbf{u}}\times\tilde{\mathbf{B}})\times\tilde{\mathbf{B}}+Kr\mathbf{f}(\tilde{\psi})\quad\text{on }\tilde{\mathcal{Q}}=\tilde{\Omega}\times(0,t_f),\end{aligned} \tag{3.4a}$$

$$\tilde{div}(\tilde{\mathbf{u}})=0\quad\text{on }\tilde{\mathcal{Q}}, \tag{3.4b}$$

$$\begin{aligned}\frac{D\tilde{\psi}}{D\tilde{t}}=&\epsilon_2\left(\eta^2\tilde{\Delta}\tilde{\psi}-\frac{\lambda_1(\tilde{c})}{\tilde{\delta}^2}g'(\tilde{\psi})-\frac{\tilde{\lambda}_2(\tilde{c})}{\tilde{\delta}}p'(\tilde{\psi})\right)\\&-\frac{\epsilon_2\left(\eta\eta''+(\eta')^2\right)}{2}\left\{2\tilde{\psi}_{xy}\sin2\theta-\tilde{\Delta}\tilde{\psi}-(\tilde{\psi}_{yy}-\tilde{\psi}_{xx})\cos2\theta\right\}\\&+\epsilon_2\eta\eta'\left\{\sin2\theta(\tilde{\psi}_{yy}-\tilde{\psi}_{xx})+2\tilde{\psi}_{xy}\cos2\theta\right\}\quad\text{on }\tilde{\mathcal{Q}},\end{aligned} \tag{3.4c}$$

$$\begin{aligned}\frac{D\tilde{c}}{D\tilde{t}}=&\tilde{div}\left(\tilde{D}(\tilde{\psi})\tilde{\nabla}\tilde{c}\right)+\tilde{div}\left(\tilde{\alpha}_0\tilde{D}(\tilde{\psi})\tilde{c}(1-\tilde{c})\left(\frac{\lambda_1'(\tilde{c})}{\tilde{\delta}}g'(\tilde{\psi})\right.\right.\\&\left.\left.-\tilde{\lambda}_2'(\tilde{c})p'(\tilde{\psi})\right)\tilde{\nabla}\tilde{\psi}\right)\quad\text{on }\tilde{\mathcal{Q}},\end{aligned} \tag{3.4d}$$

with the initial and boundary conditions

$$(\tilde{\mathbf{u}},\tilde{\psi},\tilde{c})(t=0)=(\tilde{\mathbf{u}}_0,\tilde{\psi}_0,\tilde{c}_0)\quad\text{on }\tilde{\Omega}, \tag{3.5a}$$

$$\tilde{\mathbf{u}}=0,\quad\frac{\partial\tilde{\psi}}{\partial\mathbf{n}}=0,\quad\frac{\partial\tilde{c}}{\partial\mathbf{n}}=0\quad\text{on }\tilde{\Sigma}=\partial\tilde{\Omega}\times(0,t_f), \tag{3.5b}$$

where $Pr=\mu/D_L$ is the Prandtl number, $Ra_c=g\beta_c\ell^3/D_L\mu$, is the solutal Rayleigh number, $Ha=(\sigma_e/\rho_0\mu)^{1/2}B_0\ell$ is the Hartmann number and $Kr=\alpha\ell^3/\rho_0D_L^2$, $\tilde{\delta}=\delta/\ell$ is the adimensional interface thickness, $\tilde{\lambda}_2=\ell\lambda_2$, $\tilde{\alpha}_0=\alpha_0/\ell$ and $\epsilon_2=M_\psi\epsilon_0^2/D_L$ are the adimensional parameters and $\mathbf{e}_G=(0,1)$. For model parameters, we have used physical values of the binary mixture Ni-Cu as given in Table 1 and $\mathbf{f}(\tilde{\psi})=(\tilde{\psi},\tilde{\psi})$. The density ρ, viscosity μ, and electrical conductivity σ_e are assumed to be constant in the liquid as well as in the solid, therefore we have used average values of Ni and Cu for these constants in the simulations and we define $\alpha=3.57\,10^4$. The adimensional space unit ℓ is chosen as $\ell=2.8284\times10^{-6}m$ which gives the domain length equal to 8 and the domain as $\tilde{\Omega}=[-4,4]\times[-4,4]$. With this value of ℓ, we have the adimensional $\tilde{\delta}=0.03$ which corresponds to an interface thickness δ of order $10^{-8}m$. Since the value of δ is strongly dependent on the size of mesh and as

Table 1: Physical values of constants.

Property Name	Symbol	Unit	Nickel	Copper
Melting temperature	T_m	K	1728	1358
Latent heat	L	J/m^3	2350×10^6	1758×10^6
Diffusion coeff. liquid	D_L	m^2/s	10^{-9}	10^{-9}
Diffusion coeff. solid	D_S	m^2/s	10^{-13}	10^{-13}
Linear kinetic coeff.	β	$m/K/s$	3.3×10^{-3}	3.9×10^{-3}
Interface thickness	δ	m	8.4852×10^{-8}	6.0120×10^{-8}
Density	ρ	Kg/m^3	7810	8020
viscosity	μ	$Pa\cdot s$	4.110×10^{-6}	0.597×10^{-6}
Surface energy	σ	J/m^2	0.37	0.29
Electrical conductivity	σ_e	S/m	14.3×10^6	59.6×10^6
Molar volume	V_m	m^3	7.46×10^{-6}	7.46×10^{-6}
Mode Number	k	N/A	4	4
Anisotropy Amplitude	γ_0	N/A	0.04	0.04

the mesh size should be sufficiently less than the interface thickness δ and we have used a coarse mesh for our simulations due to technical difficulties in computations, therefore we fix the value of the adimensional interface thickness as $\tilde{\delta}=0.05$ for our simulations to ensure the mesh size less than the interface thickness. The adimensional final time is $t_f=0.13$, which corresponds to the real physical final time of $T_f=1$ ms. Note that big time steps and smaller interface values can create convergence problems during the calculation of numerical solution of the problem. We choose the values of the physical constants (see Table 1) for the phase-field and concentration equations in our model as given in [34] and the constants associated with the flow equations are chosen by keeping in view the properties of substances A (Copper (Cu) in the present case) and B (Nickel (Ni) in the present case).

Nota Bene: the use of "˜" for the variables x,y and t will now be omitted.

Initially at the start of solidification, the initial condition is taken to be a circular seed (impurity) of radius 0.2 at the center of the domain $\tilde{\Omega}$ (see Fig. 4). Inside the circular seed, the value of $\tilde{\psi}$ is 0 and outside this seed the value of $\tilde{\psi}$ is 1. The concentration $\tilde{c}$ in the initial seed is equal to 0.482 and outside the seed it is taken as 0.497, i.e.,

$$\tilde{\psi}(x,y,t=0)=\begin{cases} 0, & \text{if } x^2+y^2<0.2,\\ 1, & \text{if } x^2+y^2\geq 0.2,\end{cases} \tag{3.6}$$

and

$$\tilde{c}(x,y,t=0)=\begin{cases} 0.482, & \text{if } x^2+y^2<0.2,\\ 0.497, & \text{if } x^2+y^2\geq 0.2.\end{cases} \tag{3.7}$$

Obviously, the velocity inside and outside the circular solid seed is taken to be 0 initially. The values of the initial concentration, inside and outside the initial seed, are given differ-

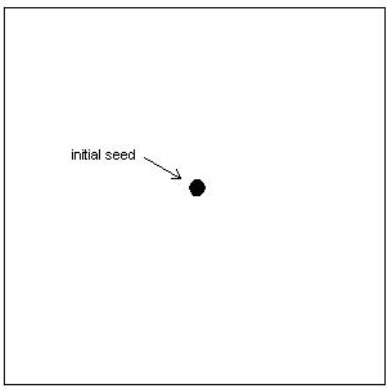

Figure 4: Geometry of the domain.

ent by different authors depending on the phase diagram of binary mixture Ni-Cu (see, e.g,. [10, 15, 34]).

3.2 Numerical scheme and implementation details

In this section we elaborate the numerical resolution of the problem (3.4). First, we discretize the problem with respect to spatial coordinates using mixed finite elements, which satisfy the InfSup condition (Babuska-Brezi's condition), for the velocity $\tilde{\mathbf{u}}$ and pressure $\tilde{p}$ in the system (3.4a)-(3.4b) and the usual finite elements for phase-field $\tilde{\psi}$ and concentration $\tilde{c}$ in the equations (3.4c) and (3.4d) respectively. More precisely we have used mixed finite elements $\mathbb{P}_i - \mathbb{P}_{i-1}$ for the velocity $\tilde{\mathbf{u}}$ and pressure $\tilde{p}$ and $\mathbb{P}_i$ for the phase-field $\tilde{\psi}$ and concentration $\tilde{c}$, respectively, where $\mathbb{P}_i$ is the polynomial of degree i. We obtain a system of nonlinear ordinary differential equations. The derived non-linear systems are then solved by using solver DASSL: for the time discretization, we have used back-ward difference Euler's formula and the resulting non-linear systems are solved using Newton method (for more details about the solver DASSL see e.g., [19]). To implement the developed method, we have employed Comsol together with Matlab tools.

Remark 3.1. Before employing the developed numerical scheme to perform numerical simulations of the model in the case of Ni-Cu, we have studied the convergence (both with respect to space and time variables) and stability of the scheme by considering several examples with known exact solutions (with parameters and data corresponding to the mixture Ni-Cu). We have demonstrated numerically that the error estimates with respect to space are of order $i+1$ for velocity $\tilde{\mathbf{u}}$, phase-field $\tilde{\psi}$ and concentration $\tilde{c}$ and of order i for the pressure $\tilde{p}$, and the error estimates with respect to time are of order 1 for $(\tilde{\mathbf{u}}, \tilde{p}, \tilde{\psi}, \tilde{c})$. The stability of the scheme has also been studied by introducing a random function, which varies between 0 and 1, in the model. We found that the numerical scheme is convergent and stable.

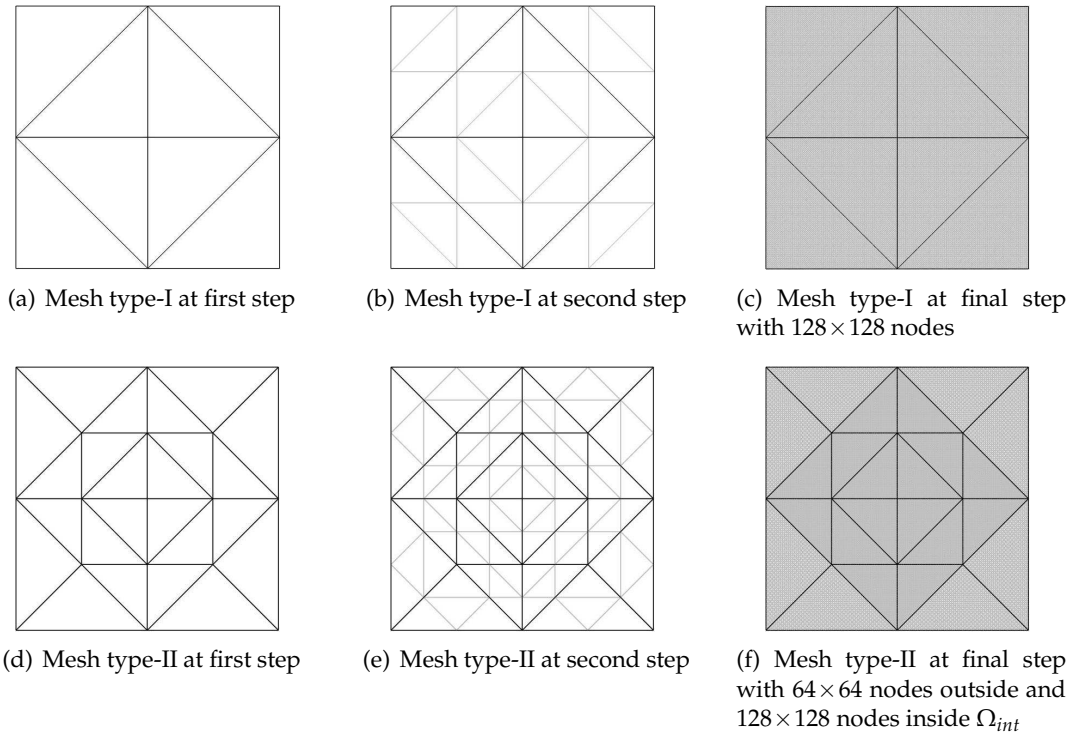

(a) Mesh type-I at first step (b) Mesh type-I at second step (c) Mesh type-I at final step with 128×128 nodes

(d) Mesh type-II at first step (e) Mesh type-II at second step (f) Mesh type-II at final step with 64×64 nodes outside and 128×128 nodes inside Ω_{int}

Figure 5: Types of mesh used in simulations.

We have used two types of structured meshes, the first type of mesh is generated in a way that first we have divided the domain, at first step, into eight triangles (see Fig. 5(a)), at second step each of these eight triangles are further divided into four triangles (see Fig. 5(b)), at third step we have divided each triangle further into four triangles and so on. The final mesh used for the simulations is shown in Fig. 5(c) in which there are 128×128 nodes containing 32768 triangular elements. The second type of mesh is generated in the similar way except that we have made a square given by

$$\Omega_{int}=\left\{(x,y)\in\mathbb{R}^2 \mid x,y \text{ belongs to square } \mathbb{S}\right\}, \tag{3.8}$$

where $\mathbb{S}=\mathbb{L}_1\cup\mathbb{L}_2\cup\mathbb{L}_3\cup\mathbb{L}_4$ such that

$$\begin{aligned}
\mathbb{L}_1&=\{(x,y)\mid y=-x+4,\ 0\le x\le 4\},\\
\mathbb{L}_2&=\{(x,y)\mid y=x+4,\ -4\le x\le 0\},\\
\mathbb{L}_3&=\{(x,y)\mid y=-x-4,\ -4\le x\le 0\},\\
\mathbb{L}_4&=\{(x,y)\mid y=x-4,\ 0\le x\le 4\},
\end{aligned}$$

inside the domain $\tilde{\Omega}=[-4,4]\times[-4,4]$ and the triangles inside Ω_{int} are divided two times greater than the triangles outside Ω_{int} (see Fig. 5). The final mesh used in simulations has 128×128 nodes inside and 64×64 nodes outside the square Ω_{int} containing 24576

triangular elements (see Fig. 5(f)). The second kind of mesh is used to save the time and to reduce memory requirement without having effect on the results.

We have used two types of finite elements to solve the problem (3.4). First is $\mathbb{P}_2-\mathbb{P}_1$ for the magnetohydrodynamic type system and $\mathbb{P}_2$ finite elements for the phase-field and concentration equations respectively. Second is the $\mathbb{P}_3-\mathbb{P}_2$ for the magnetohydrodynamic type system and $\mathbb{P}_3$ for the phase-field and concentration equations of the problem (3.4). It is important to mention that using first kind of finite elements and type-I mesh, it takes approximately 29 hours and using type-II mesh takes approximately 18 hours to complete one simulation. And using second type of finite elements with type-II mesh, it takes about 8 days to execute one simulation using the hardware defined below.

To carry out all simulations we have used a Dell Laptop computer with $4GB$ of computer memory and $2GHz$ core^2 dual processor with $64-bit$ Vista windows.

3.3 Numerical simulations

In this section, we shall present simulations of our model problem (3.4) for different cases. First, we have solved the model without magnetic-field, that is, with $\mathbf{B}=0$ and used $\mathbb{P}_2$ finite elements for the velocity $\mathbf{u}$, phase field ψ and concentration c and $\mathbb{P}_1$ for the pressure p. Type-I mesh with 128×128 nodes for 210053 degree of freedom is used in this simulation. The vector plot of velocity field are presented in Fig. 6, and plots of phase-field, concentration and their contour plots are given in Fig. 7. We notice that the magnitude of velocity is $2.8\ 10^{-6}m/s$ which is very small therefore the convection has no effect on the growth of the dendrite. The dendrite in this case is completely symmetric about x-axis and y-axis.

Second, we consider the complete set of the model equations (3.4) and present the simulations of our model by introducing different magnetic fields. To observe the effect of magnetic field on the dendrite growth, we have fixed all other parameters and solved the problem (3.4), first by choosing different constant magnetic fields at angles 90°, 45° and then introducing various variable magnetic fields both in time and spatial variables. All these simulations are performed, using $\mathbb{P}_2$ finite elements for the velocity $\mathbf{u}$, phase-

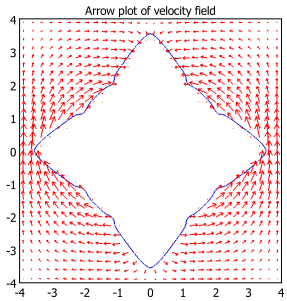

Figure 6: Vector plot of velocity field without magnetic-field $\tilde{\mathbf{B}}$.

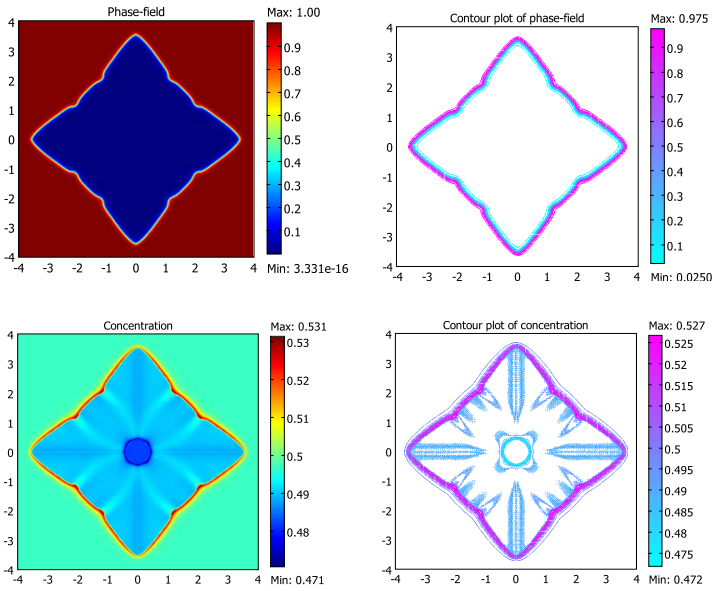

Figure 7: Phase-field, concentration and their contour plots.

field ψ and concentration c and $\mathbb{P}_1$ for the pressure p. Type-I mesh, with 128×128 nodes, is used to solve the problem in all cases.

We present the results obtained in the simulations of our model with the magnetic field at an angle 45° in the figures of the first column of Fig. 14. In this case, we remark that the magnitude of the velocity has been increased to $0.0034m/s$ and the dendrite is deformed along the direction of the applied magnetic field. We can observe that the flow behavior of the melt is also along the applied magnetic field which forces the primary arms of the dendrites to deform along the direction of magnetic field. The upper and right arms of the dendrite are smaller than the bottom and left dendrite arms. The dendrite in this case is symmetric along the line $y=x$. The deformation in the dendrite structure has been achieved by using $B_0=10$. We have noticed that with less amount of the B_0, the dendrite structure does not change considerably. This observation confirms the claim of the author of [20] who examined experimentally that one has to apply ultra-high magnitude of constant magnetic field to deform the morphology of the dendrites or a variable magnetic field should be applied to deform the structure of dendrites. To demonstrate further the authors claim, next we give the simulations by applying a variable magnetic field $\tilde{\mathbf{B}}=(\cos x,\sin y)$ in Figs. 8 and 9. In this case, we can see that the structure of the dendrite has been deformed significantly due to remarkable increase in the magnitude of the velocity to $0.016m/s$. The dendrite is no more symmetric along any of the axis. We have shown the vector plots of velocity field in Fig. 8 at time $t_f=0.125$ for the better apprehension of flow behavior of the velocity in the vicinity of the dendrite. The plot shows that the velocity along the left arm is towards the wall of the domain

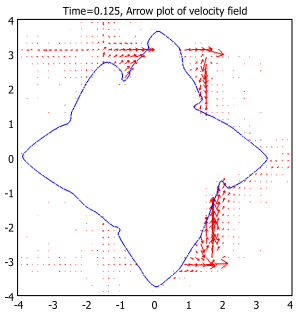

Figure 8: Vector plot of velocity field with $\tilde{\mathbf{B}}=(\cos x,\sin y)$.

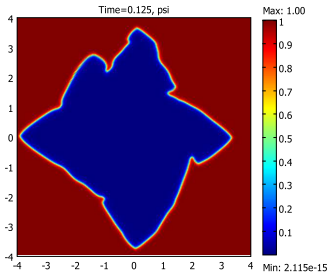

(a) Phase-field

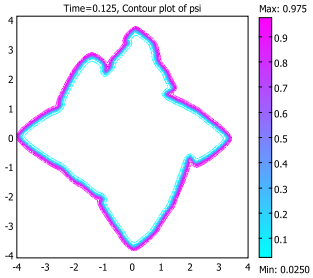

(b) Contour phase-field

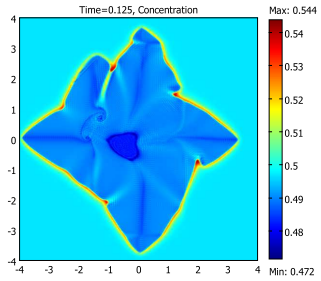

(c) Concentration

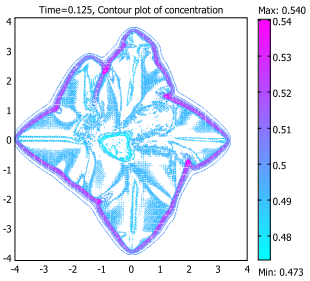

(d) Contour concentration

Figure 9: Plots of phase-field and concentration obtained for variable magnetic field $\tilde{\mathbf{B}}=(\cos x,\sin y)$ using type-I mesh and $\mathbb{P}_2$ for the velocity, phase-field and concentration and $\mathbb{P}_1$ for the pressure.

which encourages the secondary arms to grow along the left dendrite arm whereas along the right primary arm, the velocity is towards the dendrite arm which forces it to grow slowly and also restrains the secondary arms to generate along it.

Now we show the effect of magnetic field magnitude on dendrite structure. Fig. 10 shows the dendrites at a level set $\psi=1/2$ of phase-field variable for different B_0 in case of $\tilde{\mathbf{B}}=(\cos x,\sin y)$. We have noticed that with the small value of B_0, the deformation in the dendrite structure is not significant but as the amount of B_0 increases, the dendrite deforms significantly.

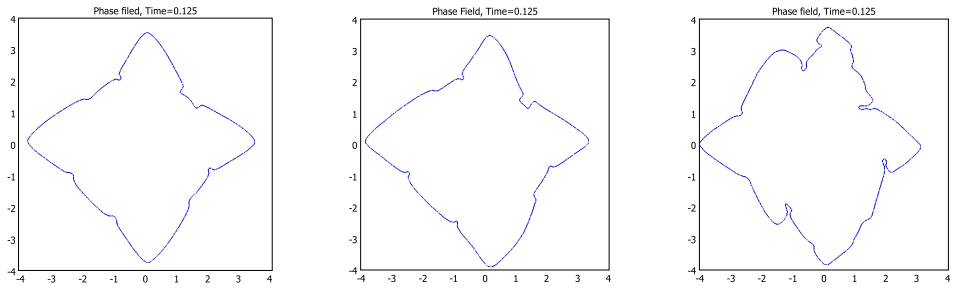

(a) $B_0=0.1T$ (b) $B_0=5T$ (c) $B_0=30T$

Figure 10: Comparison of dendrites with different B_0 in case of $\tilde{\mathbf{B}}=(\cos x,\sin y)$.

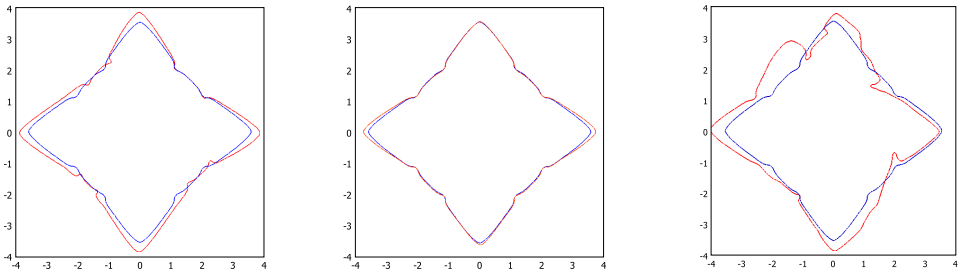

(a) $\tilde{\mathbf{B}}=\frac{1}{\sqrt{2}}(1,1)$ (b) $\tilde{\mathbf{B}}=(0,1)$ (c) $\tilde{\mathbf{B}}=(\cos x,\sin y)$

Figure 11: Comparison of dendrites without (blue curve) and with magnetic-fields (red curve), (a) $\mathbf{B}$ at 45°, (b) $\mathbf{B}$ at 90°, (c) $\mathbf{B}=(\cos x,\sin y)$.

Fig. 11 shows the comparison of the dendrites at a level set $\psi=1/2$ of the phase-field variable without and with magnetic-field at 90°, 45°, and the variable magnetic field. In Fig. 11(a), we notice that by applying magnetic-field at angle 90°, the form of dendrite has not been changed considerably, but the dendritic arms along x-axis have grown up little longer than the arms along the y-axis and it is now symmetric only about the y-axis. We have also seen this behavior of the dendrite arms by applying the magnetic field at 0° and found that in this case the dendrite arms along y-axis have grown up little larger than the dendrite arms along x-axis. Fig. 11(b) shows that by the application of magnetic-field at an angle 45°, the structure of the dendrite has been changed and the dendrite arms have grown up more rapidly and collide with the walls of the domain. The top and right arms of the dendrite are smaller than the bottom and left dendrite arms and it is now symmetric about the line $y=x$. In Fig. 11(c), we can see that the variable magnetic-field has deformed the structure of the dendrite remarkably. We found an irregular structure of dendrite in this case and the dendrite is no longer symmetric about any of axis. The left arm of the dendrite has grown up more than the right arm and they have completely different shape from other cases. We conclude from these results that the constant magnetic-field has not significant effect on the growth and structure

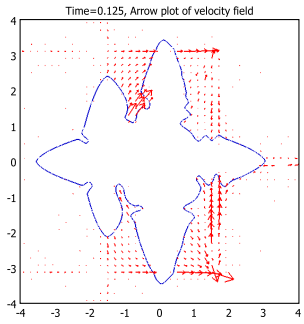

Figure 12: Vector plot of velocity field with $\tilde{\mathbf{B}}=(\cos x,\sin y)$.

of the dendrites. To deform the dendrites considerably in this case we have to apply a very strong constant magnetic field. We also notice that the variable magnetic-field have changed the form and structure of the dendrites remarkably. Our results are in good agreement with the observations made by [20], who examined the constant magnetic-field does not effect significantly the inter-dendritic flows and micro-segregations during the solidification process.

Further we have solved the model using $\mathbb{P}_3$ finite elements for the velocity, phase-

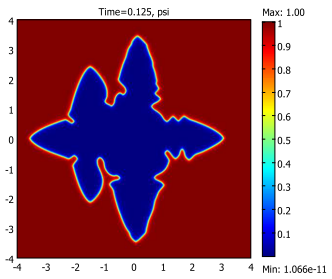

(a) Phase-field

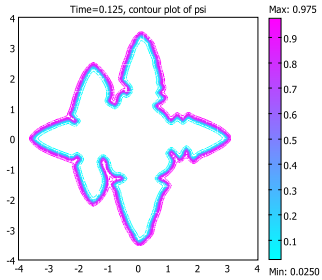

(b) Contour phase-field

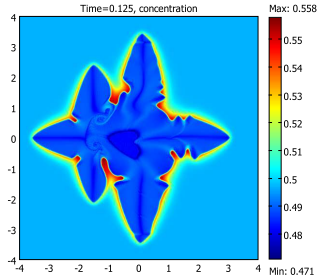

(c) Concentration

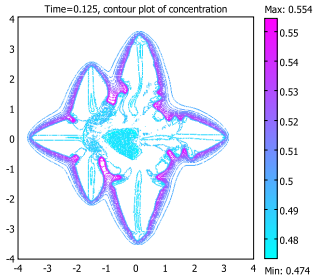

(d) Contour concentration

Figure 13: Plots of phase-field and concentration obtained for variable magnetic field $\tilde{\mathbf{B}}=(\cos x,\sin y)$ using type-II mesh and $\mathbb{P}_3$ for the velocity, phase-field and concentration and $\mathbb{P}_2$ for the pressure.

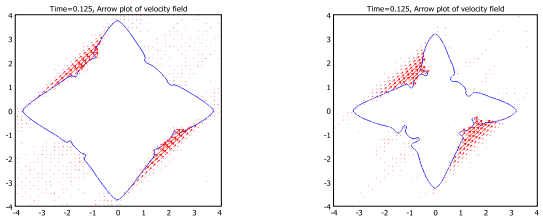

(a) Velocity field

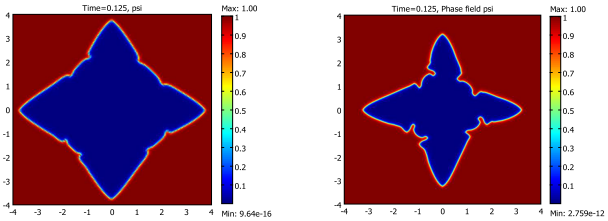

(b) Phase-field

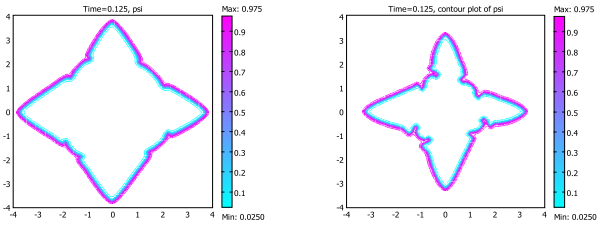

(c) Contour phase-field

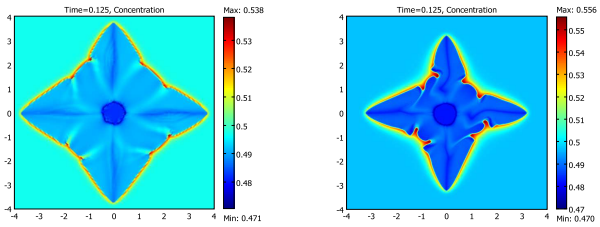

(d) Concentration

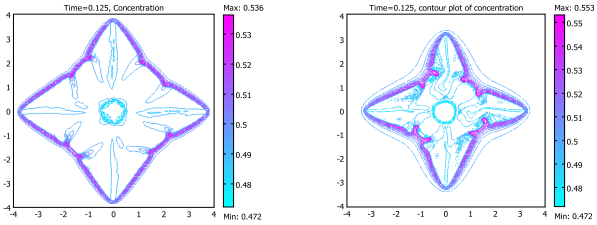

(e) Contour concentration

Figure 14: Plots of velocity, phase-field and concentration obtained for magnetic field $\tilde{\mathbf{B}}=\frac{1}{\sqrt{2}}(1,1)$ using type-I (resp. type-II) mesh and $\mathbb{P}_2$ (resp. $\mathbb{P}_3$) for the velocity, phase-field and concentration and $\mathbb{P}_1$ (resp. $\mathbb{P}_2$) for the pressure.

field and concentration and $\mathbb{P}_2$ for the pressure using type-II mesh for the magnetic-field at an angle 45° and a variable magnetic-field $\tilde{\mathbf{B}}=(\cos x,\sin y)$ and presented the results in Fig. 13 and in the second column of Fig. 14 ($B_0=10T$). We noticed that the flow patterns in these cases are similar to the previously mentioned results in Fig. 9 and in the first column of Fig. 14. The magnitude of velocity field has been increased slightly to $0.0037m/s$ in the case of magnetic-field at an angle 45° and $0.0199m/s$ for a variable magnetic-field $\tilde{\mathbf{B}}=(\cos x,\sin y)$. In Fig. 14, we observe that the dendrite is more refined and the secondary dendrite arms have also been started to grow along the primary dendrite arms. We can also see the effect of magnetic field more clearly as the top and right dendrite arms are smaller than the bottom and left dendrite arms. In Fig. 13, we can see that dendrite structure in this case has been changed significantly, large secondary arms arise along the left arm of the dendrite whereas along the other arms of the dendrite, the secondary arms have not grown up greatly.

4 Concluding remarks

In this work, we have developed a new phase-field model that incorporates convection together with the influence of the magnetic-field. For the numerical study, we have considered the case of the isothermal solidification model. The numerical simulations have been carried out by choosing the real physical parameters of the binary mixture Ni-Cu in order to fit a realistic physical alloy. We have focused mainly the effect of magnetic-field on the growth of dendrites during the solidification process by considering various magnetic-fields (all other parameters remain fixed). We have found that the constant magnetic-field does not effect considerably but the variable magnetic-field has a significant effect on the structure of dendrites and on the dynamics of the melt flow. These observations are in good agreement with the study made by [20]. The simulations can be broaden for the non-isothermal anisotropic case by the inclusion of the temperature equation.

It is clear that, due to the multi-scale nature of solidification microstructures, the number of mesh elements used in our preliminary simulations is not very sufficient to compute in a computationally efficient manner the dendritic growth, because they require very significant spatial resolution and particularly in the neighborhood of the free-phase interface which are computationally intensive and time consuming. Therefore, to get even closer to a realistic calculation, it is necessary to use in the future a more sophisticated methods which have already proven successful, such as adaptive moving mesh techniques [32] and the references therein and implicit time stepping [27] and the references therein.

In order to predict the quality of the finished product, we can also study control problems where the control function is the magnetic-field and the observation is the desired dynamics of the dendrite by using the technique developed in Belmiloudi's Book [7].

Acknowledgments

The authors are grateful to the referees for many useful comments and suggestions which have improved the presentation of this paper.

References

[1] N. Al-Rawahi and G. Tryggvason, Numerical simulation of dendritic solidification with convection: Two dimensional geometry, J. Comput. Phys., 180 (2002), 471-496.
[2] D.M. Anderson, G.B. McFadden and A.A. Wheeler, A phase-field model of solidification with convection, Physica D, 135 (2000), 175-194.
[3] E. Bansch and A. Schmidt, Simulation of dendritic crystal growth with thermal convection, EMS, Interfaces and Free Boundaries, 2 (2000), 95-115.
[4] A. Belmiloudi, Robin-type boundary control problems for the nonlinear Boussinesq type equations, Journal of Mathematical Analysis and Applications, 273 (2002), 428-456.
[5] A. Belmiloudi, Robust and optimal control problems to a phase-field model for the solidification of a binary alloy with a constant temperature, J. Dynamical and Control Systems, 10 (2004), 453-499.
[6] A. Belmiloudi and J.P. Yvon, Robust control of a non-isothermal solidification model, WSEAS Transactions on systems, 4 (2005), 2291-2300.
[7] A. Belmiloudi, Stabilization, optimal and robust control: Theory and Applications in Biological and Physical Systems, Springer-Verlag, London, Berlin, 2008.
[8] S. Bhattacharyya, T.W. Heo, K. Chang and L.Q. Chen, A spectral iterative method for the computation of effective properties of elastically inhomogeneous polycrystals, Commun. Comput. Phys., 11 (2012), 726-738.
[9] V. Galindo, G. Gerbeth, W.V. Ammon, E. Tomzig and J. Virbulis, Crystal growth melt flow previous term control next term by means of magnetic fields, Energy Conv. Manage., 43 (2002), 309-316.
[10] M. Grujicic, G. Cao and R.S. Millar, Computer modelling of the evolution of dendrite microstructure in binary alloys during non-isotheraml solidification, J. Materials synthesis and processing, 10 (2002), 191-203.
[11] M. Gunzberger, E. Ozugurlu, J. Turner and H. Zhang, Controlling transport phenomena in the Czochralski crystal growth process, J. Crystal Growth, 234 (2002), 47-62.
[12] H.B. Hadid, D. Henry and S. Kaddeche, Numerical study of convection in the horizontal Bridgman configuration under the action of a constant magnetic field. Part 1. Two dimensional flow, J. Fluid Mech., 333 (1997), 23-56.
[13] B. Kaouil, M. Noureddine, R. Nassif and Y. Boughaleb, Phase-field modelling of dendritic growth behaviour towards the cooling/heating of pure nickel, Moroccan J. Condensed Matter, 6 (2005), 109-112.
[14] A. Karma and W.J. Rappel, Quantitative phase-field modeling of dendritic growth in two and three dimensions, Physical Review E, 57 (1998), 4323-4349.
[15] D. Kessler, Modeling, Mathematical and numerical study of a solutal phase-field model, Thèse, Lausanne EPFL, 2001.
[16] J. Kim, Phase-field models for multi-component fluid flows, Commun. Comput. Phys., 12 (2012), 613-661.

[17] P. Laurençot, Weak solutions to a phase-field model with non-constant thermal conductivity, Quart. Appl. Math., 4 (1997), 739-760.
[18] M. Li, T. Takuya, N. Omura and K. Miwa, Effects of magnetic field and electric current on the solidification of AZ91D magnesium alloys using an electromagnetic vibration technique, J. of Alloys and Compounds, 487 (2009), 187-193.
[19] L.R. Petzold, A discription of DASSL: A differential/algebraic system solver, Scientific computing, IMACS Trans. Sci. Comput., (1983), 65-68.
[20] P.J. Prescott and F.P. Incropera, Magnetically damped convection during solidification of a binary metal alloy, Trans. ASME, 115 (1993), 302-310.
[21] A. Rasheed and A. Belmiloudi, An analysis of a phase-field model for isothermal binary alloy solidification with convection under the influence of magnetic field, Journal of Mathematical Analysis and Applications, 390 (2012), 244-273.
[22] J.C. Ramirez, C. Beckermann, A. Karma and H.J. Diepers, Phase-field modeling of binary alloy solidification with couple heat and solute diffusion, Physical Review E, 69 (2004), (051607-1)-(051607-16).
[23] J.C. Ramirez and C. Beckermann, Examination of binary alloy free dendritic growth theories with a phase-field model, Acta Materialia, 53 (2005), 1721-1736.
[24] J. Rappaz and J.F. Scheid, Existence of solutions to a phase-field model for the isothermal solidification process of a binary alloy, Mathematical Methods in the Applied Sciences, 23 (2000), 491-513.
[25] M. Rappaz and M. Rettenmayr, Simulation of solidification, Current Opinion in Solid State and Materials Science, 3 (1998), 275-282.
[26] J.K. Roplekar and J.A. Dantzig, A study of solidification with a rotating magnetic field, Int. J. Cast Met. Res., 14 (2001), 79-95.
[27] J. Rosam, P.K. Jimack and A.M. Mullis, A fully implicit, fully adaptive time and space discretisation method for phase-field simulation of binary alloy solidification, J. Comput. Phys., 225 (2007), 1271-1287.
[28] R. Sampath, The adjoint method for the design of directional binary alloy solidification processes in the presence of a strong magnetic field, Thesis, Cornell University USA, 2001.
[29] T. Takaki, T. Fukuoka, Y. Tomita, Phase-field simulations during directional solidification of a binary alloy using adaptive finite element method, J. Crystal Growth, 283 (2005), 263-278.
[30] X. Tong, C. Beckermann, A. Karma and Q. Li, Phase-field simulations of dendritic crystal growth in a forced flow, Physical Review E, 63 (2001), (061601-1)-(061601-16).
[31] Tonhardt R. and Amberg G., Simulation of natural convection effects on succinonitrile crystals, Physical Review E, 62 (2000), 828-836.
[32] H. Wang, R. Li and T. Tang, Efficient computation of dendritic growth with r-adaptive finite element methods, J. Comput. Physics, 227 (2008), 5984-6000.
[33] S.L. Wang, R.F. Sekerka, A.A. Wheeler, B.T. Murray, S.R. Coriell, R.J. Braun and G.B. McFadden, Thermodynamically-Consistent Phase-Field Models for Solidification, Physica D, 69 (1993), 189-200.
[34] J.A. Warren and W.J. Boettinger, Prediction of dendritic growth and microsegregation patterns in a binary alloy using the phase-field method, Acta metall. mater, 43 (1995), 689-703.
[35] M. Watanabe, D. Vizman, J. Friedrich and G. Mueller, Large modification of crystal-melt interface shape during Si crystal growth by using electromagnetic Czochralski method, J. Crystal Growth, 292 (2006), 252-256.
[36] A.A. Wheeler, W.J. Boettinger and G.B. McFadden, Phase-field model for isothermal phase transitions in binary alloys, Physical Review A, 45 (1992), 7424-7439.